Advances in Science and Technology Research Journal

Advances in Science and Technology Research Journal, 2026, 20(6), 511–527
https://doi.org/10.12913/22998624/218923
ISSN 2299-8624, License CC-BY 4.0

Received: 2026.02.07
Accepted: 2026.04.15
Published: 2026.05.01

Data-driven condition monitoring and predictive maintenance of pulse-type pneumatic conveying systems using optical fiber sensing

Yueping Guo[1], Zhen Liu[1*], Haibo Wu[1], Yi Wu[1], Zhongfu Li[2], Yin Zhang[2,3]

[1] Liuzhou Cigarette Factory, China Tobacco Guangxi Industrial Co., Ltd., 545005 Liuzhou, China
[2] School of Automation, Guangxi University of Science and Technology, 545616 Liuzhou, China
[3] Guangxi Zhuang Autonomous Region Low-altitude Unmanned Aircraft Key Technology Engineering Research Centere, Guangxi University of Science and Technology, 545616 Liuzhou, China
* Corresponding author's e-mail: zhen_liu_2026@126.com

ABSTRACT

The research demonstrates that high-frequency pulse pneumatic conveying systems are widely used for transporting the lightweight, elastic rod-shaped materials. However, the operational instability that is caused by significant pressure fluctuations, critical component wear, and material coupling frequently leads to counting errors and sudden pipeline blockages. To overcome these challenges, this paper proposed a high-precision intelligent monitoring system and a comprehensive predictive maintenance framework. The sensing unit with a 10 kHz response frequency appears to capture transient waveform features of materials. This unit examines materials moving at high velocities that exceed 15 m/s. Moreover, an adaptive Gaussian clustering algorithm is developed. This algorithm is distinct from high-latency deep learning models. The method resolves the superposition problem. Furthermore, experimental verification demonstrated that adaptive Gaussian clustering algorithm achieves identification accuracy. The accuracy is 97.8% for multi-rod coupling events with computational latency of 0.08 ms. Thus, the algorithm significantly outperforms two-dimensional convolutional neural network and support vector machine. Additionally, a composite health index model is established to quantify system degradation. Field tests indicated that composite health index logic triggers early warnings. Nevertheless, the system maintained long-term counting error below 0.01%.

Keywords: pneumatic conveying, optical fiber sensing, adaptive gaussian clustering, multi-rod coupling identification, composite health index, predictive maintenance.

INTRODUCTION

The efficient transport of lightweight, elastic rod-shaped materials in modern automated manufacturing systems – including acetate fiber filter rods, ink pen cores, and vacuum suction elements – demonstrates that these operations rely heavily on pneumatic conveying networks [1–3]. Moreover, these critical networks function as the arterial system of the production line, utilizing compressed air to propel materials through enclosed pipelines across varying distances [4–5]. Furthermore, this technology offers significant advantages in terms of space utilization and contamination control [6–8]. However, the operational stability remains a persistent challenge for these systems. Given that these flexible rods appear different from rigid heavy materials, the materials prone to erratic behaviors within the pipeline [9–10]. Nevertheless, a slight fluctuation in air pressure or minor mechanical wear in the sending unit leads to velocity decay, resulting in the piling up phenomenon that operations seek to avoid. Thus, a blockage creates consequences that extend beyond material waste [11–13]. Additionally, this necessitates time-consuming manual interventions that paralyze production workflow, creating a bottleneck that impacts overall efficiency [14–16].

Engineers have historically examined macroscopic monitoring techniques to mitigate these significant operational risks, primarily examining global airflow or the important pressure drops at key nodes [17]. However, while these established methods demonstrated effectiveness for detecting catastrophic failures, the low-frequency measurements lack critical temporal resolution to capture transient behavior of individual rods moving at high velocities [18–19]. Consequently, these approaches often fail to provide early warnings before complete blockage occurs [20]. Nevertheless, more advanced approaches attempting to employ machine vision or high-speed cameras face different limitations: the enclosed, dark nature of stainless steel pipelines and motion blur caused by high-speed transit render image-based analysis computationally expensive and often impractical for real-time industrial deployment [21]. Moreover, a specific measuring difficulty arises from the coupling phenomenon – where two or more sticky or elastic rods travel head-to-tail, mimicking a single longer object [22–24]. Given that conventional photoelectric counters or capacitive sensors are frequently deceived by this superposition, the results lead to significant accumulation errors in production statistics that distort inventory management and energy consumption data [25].

The significant research addresses that critical gap between the need for microscopic precision and the limitations of existing macroscopic sensors, moreover suggesting that this study introduces an intelligent monitoring framework specifically designed for high-frequency pulse pneumatic conveying. Furthermore, the proposed approach indicates a streamlined method that translates the physical passage of materials into high-resolution temporal pulse signals. This research deploys a custom-designed optical fiber sensing unit with a response frequency exceeding 10 kHz. Given that materials traverse the sensing cross-section, the method captures minute voltage fluctuations generated during passage. Thus, high sensitivity allows the method to treat conveying processes as sequences of decipherable time-series events. However, every variation in pulse width and interval carries diagnostic information about system health.

Therefore, a novel multi-rod coupling identification algorithm that analyzes the statistical distribution of pulse widths to disentangle overlapping signals is developed, which can effectively resolve the counting inaccuracies that plague traditional sensors and maintaining a long-term counting error below 0.01%. Beyond quantification, a dynamic health state model was established, which correlates subtle deviations in pulse characteristics – such as broadening pulse widths or irregular intervals – with physical degradation mechanisms like pipeline leakage or sender wear. This enables the system to forecast potential blockages and trigger maintenance alerts during the sub-health operation phase, long before a breakdown occurs. The subsequent sections of this paper will detail the signal acquisition principles, derive the mathematical framework for coupling identification, and finally demonstrate the system's robustness through experimental validation in an actual industrial production environment.

The main novelties of this work are articulated across three key methodological and practical advancements. First, the study proposes an adaptive Gaussian clustering scheme specifically tailored for pulse-type pneumatic conveying signals. This method updates the cluster structure online to effectively accommodate non-stationary background noise and operational drift. Second, the research develops a novel feature-to-health mapping framework. This framework integrates time-domain pulse descriptors and statistically normalized distances into a composite health index (CHI), which is specifically designed to facilitate early anomaly escalation. Finally, the work presents an end-to-end, high-frequency optical-fiber-sensing implementation. This system was rigorously validated during a 30-day continuous operation, thereby demonstrating substantial practical value for predictive maintenance well beyond conventional offline demonstrations.

SYSTEM ARCHITECTURE AND SENSING PRINCIPLE

Physical layout and pneumatic dynamics

The experimental setup mimics a typical industrial application, functioning as the significant high-speed arterial system of a critical production line, as shown in Figure 1.

Moreover, the core conduit is constructed from stainless steel pipelines tailored to facilitate the important transport of lightweight, elastic cylindrical materials – specifically, rods with a nominal diameter of 8 mm and length of approximately 100 mm, e.g. acetate fiber filters

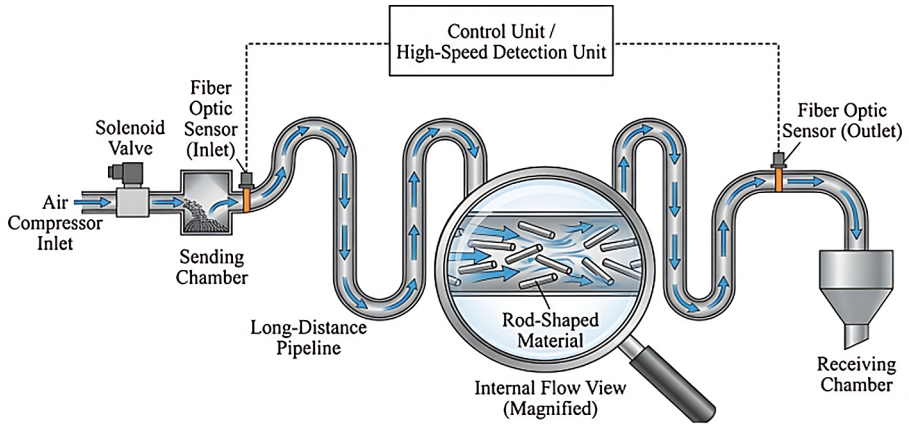

Figure 1. Schematic diagram of the high-frequency pneumatic conveying system

or ink cores. Materials are propelled by compressed air pulses regulated at 0.6 MPa. Given that the elastic nature of rods differs from rigid projectiles, the materials is susceptible to slight deformation and velocity fluctuations as they traverse complex routing paths, which exceeds 50 meters and include varying curvature radii. Therefore, this dynamic environment necessitates a monitoring solution that is non-intrusive yet sensitive enough to detect motion without disrupting the airflow field.

High-response optical sensing unit

The custom-designed through-beam optical fiber sensing mechanism enables the system to capture the transient behavior of materials that move at velocities where conventional visual observation blurs the critical details. However, conventional photoelectric switches suffer from hysteresis, whereas the sensing unit demonstrates that it is engineered for extreme temporal resolution. The optical probes are embedded at critical nodes, specifically at entry and exit points, and the probes project a collimated beam across the pipe's cross-section, as depicted in Figure 2. Moreover, the choice of optical fiber appears deliberate in that it isolates the electronic processing unit from the vibration and electromagnetic interference typical of pipeline environments while maintaining a compact footprint. Given that the detection circuit operates with a response frequency exceeding 10 kHz, the system demonstrates temporal resolution is 0.1 ms. This capability merely represents a technical specification but indicates a prerequisite for distinguishing closely spaced materials in high-density pulse streams.

To address the high-frequency mechanical vibration interference in pneumatic conveying pipelines, this study employed an adaptive notch filter during the signal preprocessing stage. During periods with no material flow, the optical fiber sensor exhibits a stable quiet period, which is exploited to identify the dominant frequency component of background mechanical noise in real time. An adaptive notch filter is then applied: the identified noise component is inverted and superimposed onto the raw signal for active cancellation. This preprocessing step improves the system's signal-to-noise ratio (SNR) by 12 dB during the peak material-transportation phase.

Signal modulation and pulse formation mechanism

The fundamental principle of data acquisition suggests that the modulation of light intensity by the passing material provides the critical basis for measurement. In the absence of material, the receiver captures a full intensity signal, maintaining a high voltage baseline. As a rod enters the sensing zone, it appears to behave as an opaque obstruction, sharply attenuating the optical signal and creating a distinct voltage drop. This transition generates a square-wave pulse in the time domain, effectively translating the physical presence of the rod into a digital footprint. Thus, the pulse provides a measurable signal that indicates material presence.

Given that the morphology of this pulse – specifically its width (T_w) – is the primary variable of interest, the mathematical relationship between the rod effective length and the velocity v that this rod passing the sensor demonstrates significant

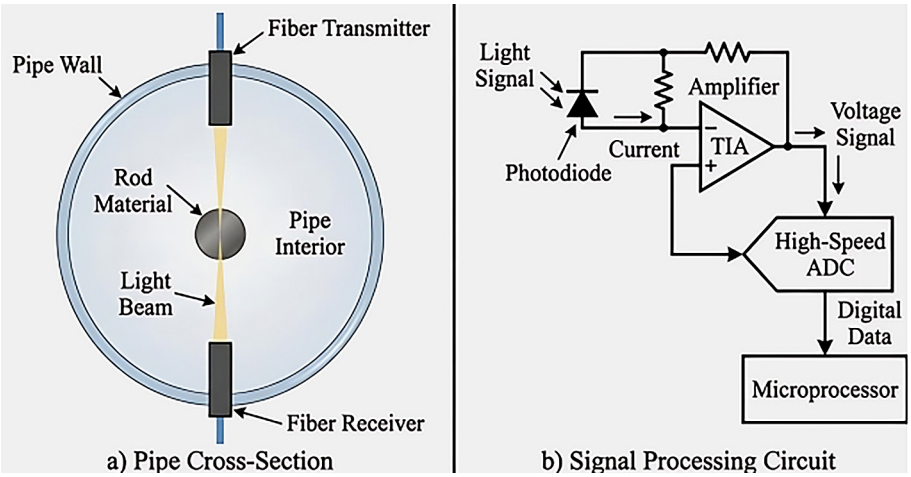

Figure 2. Detailed cross-section of the optical sensing node and signal acquisition circuit

implications for velocity measurement. Mathematically, if the effective length of the rod is L and it passes the sensor at a velocity v, the idealized pulse width is given by $T_w \approx L / v$. Nevertheless, in real-world scenarios, this relationship appears to be nuanced by the rod's elasticity and the specific beam width of the sensor. In fact, the pulse width serves as a direct, inverse proxy for conveying velocity. In light of the observed patterns, a healthy transport event is characterized by a stable, narrow pulse, whereas a widening pulse indicates velocity decay – a potential precursor to blockage, as presented in Figure 3. Digitizing these analog optical interruptions can allow the system to construct a time-series profile, which can depict the entire production flow effectively.

RECURSIVE SIGNAL PROCESSING AND FEATURE SPACE CONSTRUCTION

Adaptive baseline filtering and noise suppression

The optical receiver can capture raw analog signals that appear to be contaminated by high-frequency electromagnetic noise and slow-varying baseline drifts caused by dust accumulation on lens surfaces. Conventional monitoring methods typically rely on a static voltage threshold V_{th} to trigger counting events [26]. However, in long-term industrial operations, this rigid approach is prone to false negatives when signal amplitude degrades [27]. To address this challenge, a dynamic baseline estimation strategy coupled with a recursive moving average filter is proposed in this research.

The discrete voltage sequence sampled at 10 kHz, $S_{raw}(t)$, is denoted as the primary signal input. Furthermore, the instantaneous baseline $B(t)$ represents the empty pipe state, which is updated recursively only when no material is detected. To enhance the signal-to-noise ratio (SNR) while preserving the sharp edges of the pulse, a sliding window smoothing function is defined as follow:

$$S_{smooth}(t) = \frac{1}{N}\sum_{k=0}^{N-1} S_{raw}(t-k) \tag{1}$$

Given that noise suppression must be balanced with phase delay, the window size N is empirically set to 5 samples (0.5 ms). The adaptive triggering threshold $V_{trigger}(t)$ is not fixed but floats relative to the dynamic baseline:

$$V_{trigger}(t) = \alpha \cdot B(t) \tag{2}$$

Thus, the modulation depth coefficient α typically ranges from 0.6 to 0.8. This adaptive mechanism ensures that the system maintains detection sensitivity even if optical transmittance drops by 30%, a significant improvement in robustness compared to static comparators. To prevent the recursive updating mechanism from mistakenly identifying the long-term degradation trend as a normal baseline shift, the algorithm has added a degradation rate threshold (Δ_{deg}). When the average slope of the CHI index within the sliding window exceeds the critical value, the baseline update program is automatically suspended, the current fault characteristics are locked, and a 'potential deterioration warning' is triggered, thereby avoiding the system's adaptive 'dilution' of long-term faults.

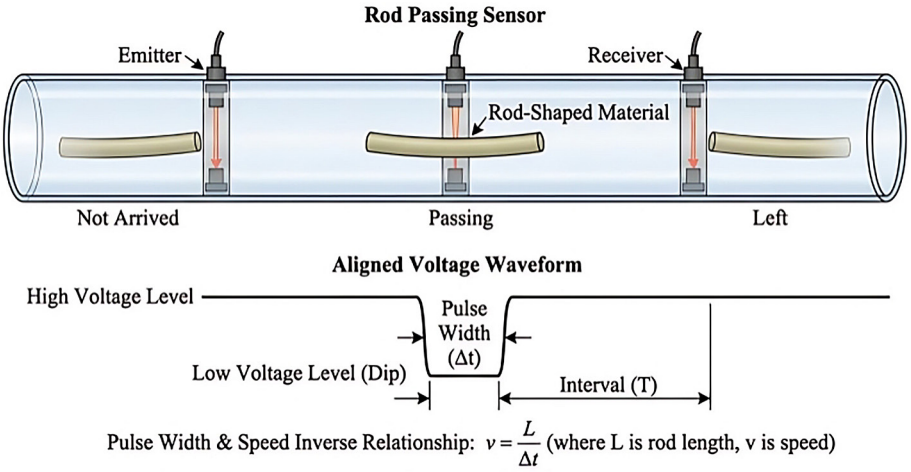

Figure 3. Rod passing sensor and voltage waveform

Hysteresis-based pulse segmentation logic

The conversion of the analog waveform into discrete logical events requires that the precise identification of the start moment (t_{start}) and the critical end moment (t_{end}) of rod passage be established. Given that the filter rods demonstrate elastic properties, the leading edges and the trailing edges of the signal exist high-frequency jitter, which deceives standard zero-crossing detectors into registering multiple counts for a single object.

Therefore, a digital hysteresis logic with dual thresholds appears necessary to eliminate this ambiguity: a lower threshold (V_L) for engaging the trigger and an upper threshold (V_H) for releasing it. The binary state of the conveyor is determined by:

$$D(t) = \begin{cases} 1 \text{ (Occupied)}, & \text{if } S_{smooth}(t) < V_L \\ 0 \text{ (Empty)}, & \text{if } S_{smooth}(t) > V_H \\ D(t-1), & \text{otherwise} \end{cases} \quad (3)$$

where: $D(t) = 1$ – rod presence blocks the beam. This locking mechanism prevents logical state oscillations due to edge noise, ensuring each physical rod corresponds to exactly one continuous low-level pulse.

Feature vector extraction and physical mapping

Once the effective pulse duration is segmented, the system extracts a multi-dimensional feature vector sequence. For the i-th detected object, the important vector is defined as:

$$\mathbf{F}_i = [T_{w,i}, T_{\text{interval},i}, A_{\text{dip},i}]^T \quad (4)$$

Given that the structural framework has been established, the components are defined physically as follows.

1. Pulse Width ($T_{w,i}$): The significant time duration for which the rod obstructs the optical path is calculated as. Furthermore, this is the critical geometric descriptor. Assuming the rod moves at a quasi-constant velocity during the transit event, the relationship between time and space is governed by:

$$v_i = \frac{L_{\text{rod}} + w_{\text{beam}}}{T_{w,i}} \quad (5)$$

where: L_{rod} – the nominal length of the material (e.g., 100 mm), w_{beam} – the effective diameter of the optical beam.

2. Pulse Interval ($T_{\text{interval},i}$): The temporal gap between the trailing edge of the i-th rod and the leading edge of the i-1-th rod can be examined.

$$T_{\text{interval},i} = t_{\text{start},i} - t_{\text{end},i-1} \quad (6)$$

where: $t_{\text{start},i}$, $t_{\text{end},i}$ – the state and the end moments of $T_{\text{interval},i}$. This variable inversely reflects instantaneous transport density.

3. Modulation Amplitude ($A_{\text{dip},i}$): $A_{\text{dip},i}$ is defined as the integral of the voltage drop, representing the energy of the blockage. An abrupt decrease in often indicates a semi-transparent foreign object or a tilted rod allowing light leakage.

Innovation in handling variable velocity

Existing counting methods demonstrates a significant limitation in the assumption of constant conveying velocity. In fact, in pulse

pneumatic systems, air expansion indicates that velocity appears to pulsate, as shown in Figure 4. The feature extraction framework accounts for this by normalizing pulse width against local average velocity trend. The velocity consistency factor (λ_i) is defined as:

$$\lambda_i = \frac{T_{w,i}}{\bar{T}_{w,\text{local}}} \quad \text{where}$$
$$\bar{T}_{w,\text{local}} = \frac{1}{k}\sum_{j=1}^{k} T_{w,i-j} \tag{7}$$

Given that the system monitors, the effect of system-wide speed fluctuations is decoupled from individual material anomalies, where λ_i deviates significantly. This normalization proves pivotal for the subsequent coupling identification algorithm, distinguishing the proposed approach from simple time-of-flight counters.

PROBABILISTIC MODELING AND MULTI-ROD COUPLING IDENTIFICATION

Stochastic superposition of pulse signals

The turbulent environment of high-pressure pneumatic pipelines at 0.6 MPa indicates that the flexible nature of the rods introduces a significant stochastic element to their critical spatial alignment. Moreover, friction variability and the local pressure gradients suggest trailing rods accelerate and latch onto leading rods. Thus, head-to-tail coupling chains are formed. Given that conventional sensors examine these composite entities, the sensor presents the entity as a single elongated pulse. However, the pulse appears indistinguishable from a slow-moving individual unit. In light of the pulse width measurements, a pulse width of $T \approx 20$ ms indicates a single rod moving at 5 m/s. However, a pulse width of $T \approx 20$ ms also suggests two coupled rods moving at 10 m/s. The ambiguity is not merely a counting task but also represents a significant statistical pattern recognition problem. Therefore, identifying the underlying multimodal distribution of the pulse stream is required [28].

Adaptive statistical baseline construction

The system must first establish a robust definition of a standard single unit under current operating conditions to disentangle these coupled signals. It is assumed that the temporal width of single rods T_w follows a Gaussian distribution $\mathsf{N}(\mu_s, \sigma_s^2)$, which is governed by the inherent velocity fluctuations of the airflow. Although the basic model is based on the Gaussian assumption, considering that the material turbulence cause the distribution of the peak signal to be skewed, the system incorporates a skewness-kurtosis test. When the signal significantly deviates from the normal distribution, the dynamic confidence interval is adjusted from 3 σ_s to a percentile interval based on kernel density estimation to ensure the accuracy of counting under complex material components.

The proposed method employs a Recursive Estimator that updates the baseline. The pulse width $T_{w,k}$ and variance μ_k after the k-th valid

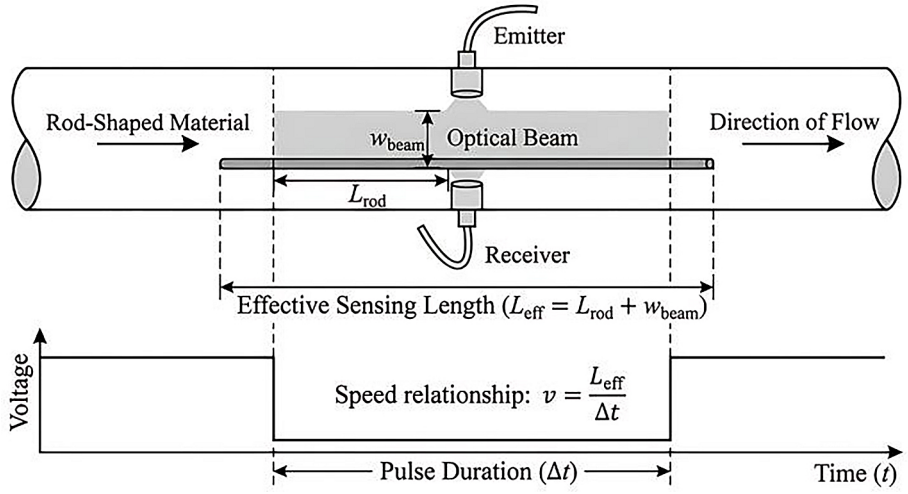

Figure 4. Visualization of the feature space

single event are denoted. The update laws establish fundamental relationship between estimated mean pulse width and the variance, which is defined as follow.

$$\mu_k = (1-\beta)\cdot\mu_{k-1} + \beta\cdot T_{w,k} \tag{8}$$

$$\sigma_k^2 = (1-\beta)\cdot\sigma_{k-1}^2 + \beta\cdot(T_{w,k}-\mu_k)^2 \tag{9}$$

Furthermore, the forgetting factor ($\beta \in (0,1)$ is set to 0.05. Thus, the model adapts to drifts in pressure while ignoring outliers. This mechanism ensures the baseline variance (μ_s) remains accurate even if speed shifts due to cycling or clogging.

Unlike traditional Gaussian mixture models that rely on static parameters, the proposed adaptive Gaussian clustering dynamically adjusts its threshold bounds continuously based on real-time streaming data. This dynamic adaptability significantly enhances the robustness of multi-rod coupling identification under varying operational conditions.

Multi-modal quantization logic

The adaptive baseline analysis suggests that a quantized multiplier model can be developed for these significant experimental observations. The fundamental hypothesis indicates that a pulse width observed from a coupling of n rods is simply be additive, but appears to be modulated by a coupling coefficient (γ) accounting for the slight overlaps or gaps at contact points. Moreover, the predicted width for n rods is given by Equation 10

$$\hat{T}_n = n\cdot\mu_s\cdot\gamma + \text{ň} \tag{10}$$

where: ň – random noise. In light of these theoretical findings, a maximum likelihood-based discriminant function is utilized to identify rod number contained within an observed pulse, derived from the Z-score distance measure.

$$Z_n = \frac{|T_{\text{obs}} - n\cdot\mu_s|}{\sigma_s} \quad \text{for} \quad n \in \{1,2,3,\ldots\} \tag{11}$$

The decision rule selects the integer n that minimizes this statistical distance, provided the result falls within a dynamic confidence interval.

$$N_{\text{count}} = \arg\min_n(Z_n) \quad \text{s.t.} \quad Z_n < \kappa \tag{12}$$

In this inequality, κ is the tolerance threshold, typically $\kappa = 3$ for a 99.7% confidence level. If the minimal Z_n exceeds κ, the pulse is flagged as an anomaly, e.g. a foreign object or a shattered rod, rather than a valid production unit, triggering a specific alarm. Flowchart of the multi-rod coupling identification algorithm is depicted in Figure 5.

Handling velocity-coupling ambiguity

A critical flaw in traditional time-of-flight counters is the inability to distinguish between a slow single rod and a fast coupled pair. It is overcame by integrating the pulse interval (T_{interval}) into the decision matrix.

Physical constraints dictate that coupled rods travel with a near-zero interval between their constituent units, $T_{\text{interval}} \to 0$ internally, but observed

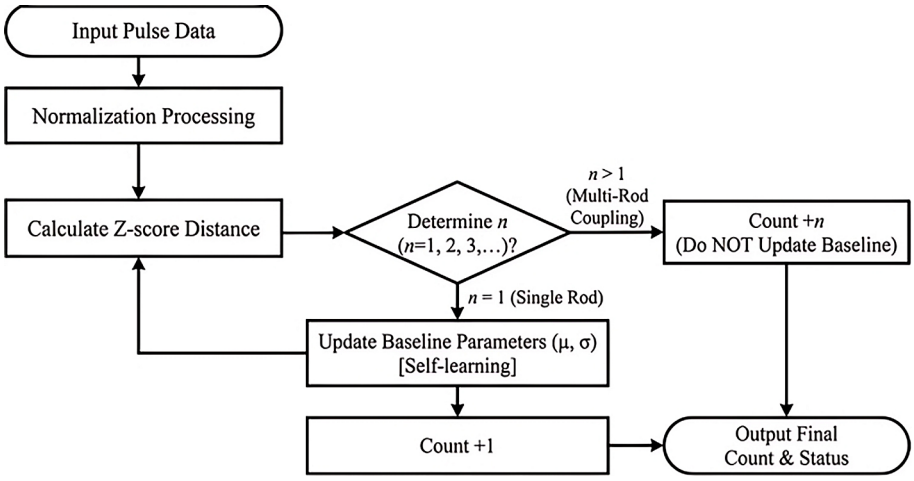

Figure 5. Flowchart of the multi-rod coupling identification algorithm

as one long pulse. Conversely, a slowing rod usually implies system-wide deceleration, which would statistically increase the gaps between all subsequent rods.
The global consistency index is defined as:

$$\Omega = \frac{T_{\text{curr}}}{T_{\text{interval}}} \tag{13}$$

where: T_{curr} – current temporal length of the passing material.

Moreover, when the consistency index demonstrates sudden spikes while the significant surrounding velocity field appears to remain relatively constant, the proposed method can reasonably weight the observed probability heavily towards the critical coupling event rather than towards a simple speed drop. Thus, this multivariate fusion can drastically reduce false positives. Additionally, the developed method can enable achievement of the reported 0.01% counting accuracy. This accuracy occurs even under unstable pressure conditions.

DYNAMIC HEALTH STATE MODELING AND PREDICTIVE MAINTENANCE STRATEGY

From passive counting to active prognostics

A precise counting serves immediate production logistics. The deeper value of the captured pulse stream indicates that it reveals the invisible degradation of the pneumatic infrastructure. In a closed loop conveying system, the mechanical anomalies, such as the gradual loosening of pipeline coupling or the abrasive wear of sending unit seals, does not manifest as sudden failures. Nevertheless, anomalies appear as subtle, progressive distortions in material kinematic fingerprint. Given that traditional pressure switches only toggle when catastrophe, e.g. blockage, has already occurred, the developed method can treat conveying velocity and interval consistency as continuous random variables. Thus, the proposed method can mine them to forecast breakdowns before disruptions occur in production schedule.

Mathematical formulation of conveying stability

To quantify system health, a sliding time window W of length K, e.g. the last 1000 rods, is established. Within this window, two critical statistical descriptors that correlate directly with physical fault mechanisms is extracted.

1. Velocity retention ratio (η_v)

A drop in air pressure due to leakage directly reduces the kinetic energy transfer. η_v is defined as the ratio of current mean velocity to the calibrated baseline velocity v_{ideal}, learned during initial healthy operation.

$$\eta_v(t) = \frac{L_{\text{rod}}}{v_{\text{ideal}}} \cdot \left(\frac{1}{K} \sum_{j=0}^{K-1} \frac{1}{T_{w,t-j}} \right) \tag{14}$$

As leakage worsens, pulses widen, driving η_v below 1.0.

2. Dispersion coefficient (ξ_{stab})

Ideally, pulses should arrive rhythmically. Mechanical friction or erratic airflow causes stuttering. This instability is measured using the coefficient of variation (CV) of the pulse intervals.

$$\xi_{\text{stab}}(t) = \frac{\sqrt{\frac{1}{K-1} \sum_{j=0}^{K-1} (T_{\text{interval},t-j} - \bar{T}_{\text{interval}})^2}}{\bar{T}_{\text{interval}}} \tag{15}$$

where: $\bar{T}_{\text{interval}}$ – the estimated mean for all $T_{\text{interval},t-j}$ ($j \in [0, K-1]$).

An increasing ξ_{stab} indicates the onset of stop-and-go motion, a strong precursor to material piling using coupling.

Construction of the composite health index

Existing methods often struggle to balance sensitivity and false alarm rates because they monitor single parameters in isolation. A fused composite health index (C_{CHI}) is introduced to integrate the aforementioned indicators into a normalized score ranging from 0 to 1. The degradation function is modeled as:

$$C_{\text{CHI}}(t) = 1 - \begin{pmatrix} \omega_1 \cdot \psi(\eta_v(t)) + \\ + \omega_2 \cdot \phi(\xi_{\text{stab}}(t)) \end{pmatrix} \tag{16}$$

where: ω_1 and ω_2 – weighting factors determined by the specific material fragility.

For example, $\omega_1 = 0.6$ for pressure-sensitive filters. $\Psi(\cdot)$ is a penalty function for velocity loss, specifically designed as exponential to reflect the accelerating risk of blockage at lower speeds. $\phi(\cdot)$ is a linear normalization of variance. To eliminate

the subjectivity in weight selection, this study introduced the Discrepancy Response Ratio (DRR) analysis. Through experimental simulation of different wear levels, the derivatives of η_v and ξ_{stab} with respect to the initial failure were quantified. For brittle materials (easily broken and prone to local blockage), the weight of ω_2 was increased to capture the waveform discreteness characteristics. For high-viscosity materials, the weight of ω_1 was increased to monitor the air pressure leakage. Finally, ω_1 and ω_2 were determined through the initial least squares regression of the system deployment.

This formula ensures that the CHI drops slowly during early wear but plummets rapidly as the system approaches the critical localized clogging velocity, as presented in Figure 6.

Although the formulation of the CHI incorporates empirical weighting to balance multi-dimensional features, its core relies on objective physical proxies: kinetic energy transfer and boundary friction disorder. To evaluate parameter robustness, a sensitivity analysis indicates that the framework remains highly stable under varying operational conditions, largely due to its dynamic baseline updating mechanism. As long as the base structural parameters are appropriately set, such as the modulation depth coefficient being maintained between 0.6 and 0.8, the CHI successfully maintains its diagnostic sensitivity even if absolute optical transmittance experiences long-term degradation. Furthermore, the proposed CHI exhibits excellent transferability to other pneumatic conveying systems and materials with different dimensions or stiffness. Because the CHI evaluates the relative deviation from an established healthy baseline rather than relying on absolute rigid thresholds, transferring the system to a new material only requires a brief initial calibration phase. During this phase, the system processes a sample of normal flow data to extract new nominal pulse width and energy baselines. Once recalibrated, the identical CHI formulation can directly monitor the new material flow without requiring architectural modifications to the underlying algorithm.

Self-learning state classification and logic

The self-learning capability of the system is realized through an unsupervised clustering process. During the commissioning phase, first 24 hours, the system collects feature vectors to construct a distribution of the healthy domain. Based on the statistical boundaries of this domain, the operational status is dynamically categorized into three zones.

1. Zone I: Stable operation ($C_{CHI} > 0.85$). The system operates within design specifications. No action is required.
2. Zone II: Sub-health/maintenance warning ($0.60 < C_{CHI} \leq 0.85$). This is the key innovation zone where predictive maintenance occurs.
   - Scenario A: If η_v drops but ξ_{stab} remains stable, the logic infers pneumatic leakage or compressor fade, prompting a check of gaskets and valves.
   - Scenario B: If ξ_{stab} spikes while velocity is normal, it suggests mechanical friction or material deformation, advising inspection of pipeline joints or bends.
3. Zone III: Critical alarm ($C_{CHI} \leq 0.85$).

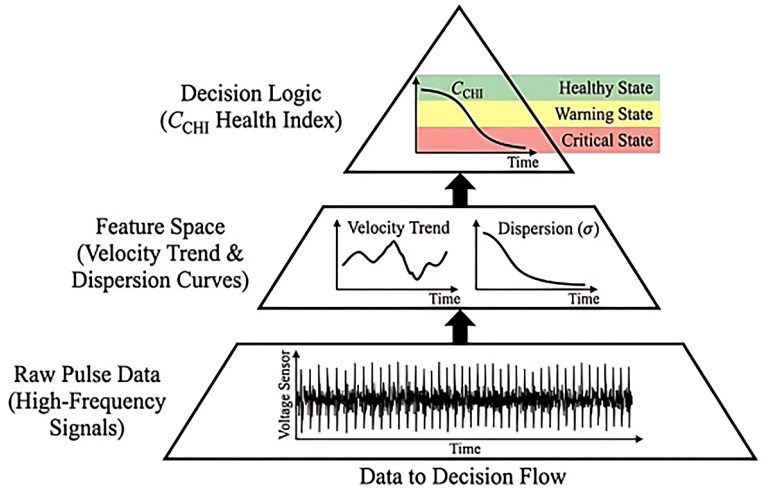

Figure 6. Architecture of the health state model

The risk of blockage is imminent. The system issues a high-level alert to stop feeding material before the pipe becomes completely impacted, saving hours of manual unclogging time. The degradation trend is depicted in Figure 7, in which real-world data showing the CHI curve declining 2 hours prior to a potential blockage event.

Key algorithmic parameters

To bridge the conceptual design of the proposed framework with its practical software implementation, and to ensure full reproducibility of the real-time monitoring system, Table 1 summarizes the core algorithmic parameters utilized in this study. The listed values represent the optimized configuration established during the initial 24-hour self-learning calibration phase and were consistently applied throughout the experimental validation.

EXPERIMENTAL VERIFICATION AND APPLICATION

The proposed detection system was integrated into a full-scale industrial prototype to test its effectiveness. In the test process, the proposed method was tested under conditions that mimicked the chaotic reality of a factory floor–varying pressures, mechanical wear, and high-speed throughput – and to quantitatively benchmark it against state-of-the-art methods found in recent researches. These conditions can demonstrate the proposed method's practical capabilities, which provides support for operational feasibility for the proposed method.

Experimental setup and environmental constraints

The test bed was constructed using a stainless steel pipeline network exceeding 50 m with multiple 90-degree bends that simulated the complex factory routing conditions. The standard acetate fiber filter rods – diameter 8 mm, length 100 mm – were utilized as the significant transport material, driven by a compressed air system that was regulated at 0.6MPa. The data acquisition core consisted of high-speed optical fiber sensors positioned at the critical junctions. These sensors feed into the custom detection unit, which boasts a response frequency of 10 kHz and latency of less than 0.1 ms. Furthermore, high temporal resolution appears non-negotiable. At industrial speeds, a double-rod coupling event passes the sensor window in mere milliseconds, requiring the system capture the subtle waveform distortions that distinguish a single rod from a pair.

Three controlled disturbances were introduced in this research to strictly evaluate the robustness of the proposed method. Given that pressure variations can be used to demonstrate significant effects for the proposed method, the supply pressure was randomly varied between 0.4MPa and 0.7MPa to alter the rod velocity. Furthermore, simulated leakage involved a bypass valve that was opened incrementally to simulate seal aging, dropping effective transport force. Coupling injection also involved manually feeding rods in head-to-tail configurations. $n = 2$ and $n = 3$ events were forced.

The composition schematic diagram and the setup of the test platform are depicted in Figure 8 and Figure 9, respectively. In light of the sensor

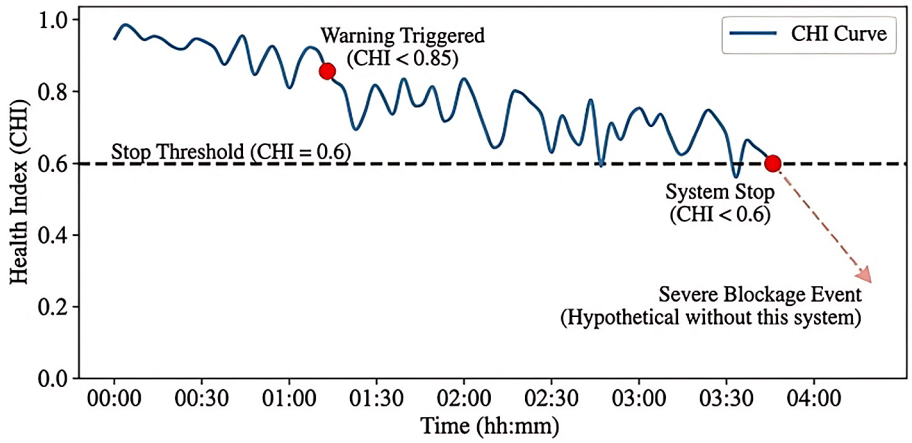

Figure 7. The degradation trend

Table 1. Summary of key algorithmic parameters

Physical definition / Description of parameters	Typical value / Range
Sampling frequency of the data acquisition system	10 kHz
Sliding window size for real-time signal processing	1000 samples (0.1 s)
Signal intensity threshold for pulse event segmentation	Dynamically updated (default ≈0.5)
Modulation depth coefficient for baseline stability	0.6~0.8
Effective width of the optical beam	5 mm
Weighting coefficients for CHI calculation	α=0.6, β=0.4
Time interval for dynamic baseline updating	3600 s (1 hour)

topology requirements, Figure 9 highlighted the significant sensor topology and the signal flow from the physical pipeline to the digital processing unit that demonstrates the complete detection pathway.

Comparative analysis with state-of-the-art methods

The proposed adaptive gaussian clustering (AGC) is benchmarked against three significant competing methodologies that are cited in recent high-impact instrumentation research. Fixed thresholding (FT) represents a traditional method that relies on static pulse-width limits. SVM-based classification (SVM-C) is a machine learning approach using support vector machines for pattern recognition. Two-dimensional convolutional neural network (2D-CNN) is a deep learning model optimized for time-series signal classification.

The evaluation was conducted on a total of N = 50,000 segmented conveying events extracted from the high-frequency optical-fiber sensing stream. each event corresponds to one detected pulse window after preprocessing and event segmentation.

Table 2 summarizes the dataset used for evaluation, including the total number of segmented events and the distribution across rod-count classes. The class labels follow the experimental definition of single-rod (n = 1), double-rod (n = 2), and triple-rod (n = 3) conveying events. All reported classification metrics in this research are computed using these labeled events.

The comparison presented in Table 3 focused on two critical metrics, identification accuracy specifically for multi-rod events and computational latency are crucial for real-time loops.

The data in Table 3 indicated that while CNN demonstrates exceptional accuracy for single rods, the significant computational weight creates a critical bottleneck, potentially missing the incoming signals during high-throughput bursts. The proposed AGC method can strike an optimal balance. Additionally, the proposed method is highly efficient, achieving an average computational latency of merely 0.08 ms per event. To ensure transparency regarding this real-time capability, all computational performance tests were executed on an industrial computing platform equipped with an Intel Core i7-10700K CPU at 3.80 GHz and 16 GB of RAM, running a 64-bit operating system without GPU acceleration. It is important to emphasize that this 0.08 ms latency strictly encompasses the complete processing pipeline for a single segmented pulse window, including signal preprocessing such as filtering and real-time background noise cancellation, feature extraction involving computation of dynamic properties such as pulse width, peak

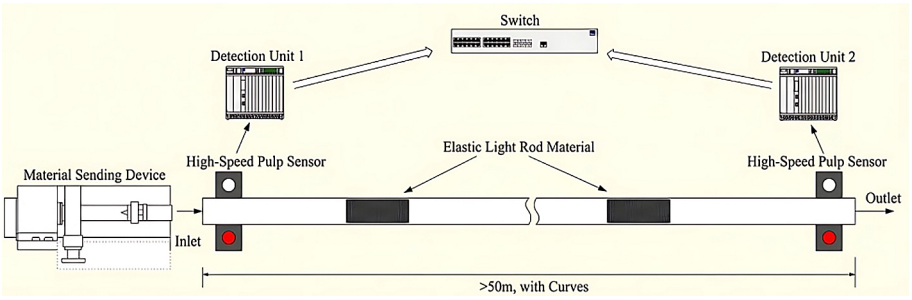

Figure 8. Schematic diagram of the composition of the detection device

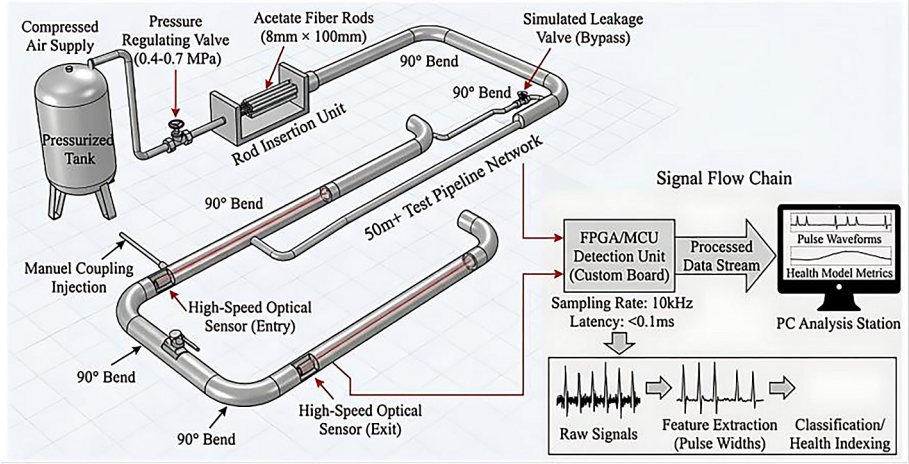

Figure 9. A 3D setup schematic of the test platform

Table 2. Dataset sizes and class distributions used for evaluation

Class (rod count)	Events	Percentage (%)
n=1 (single-rod)	20,000	40
n=2 (double-rod)	15,000	30
n=3 (triple-rod)	15,000	30
Total	50,000	100

amplitude, and total energy, and the final decision logic comprising classification and thresholding. This extremely low processing overhead, requiring only standard CPU resources, effectively guarantees continuous, zero-bottleneck monitoring of the high-frequency optical-fiber sensing stream.

Complex flow analysis and robustness

The significant algorithmic stability for methods was visualized through the plotting of probability density evolution for the detected pulse widths under varying velocity conditions. The data separation capability of 2D-CNN and the proposed method is displayed in Figure 10. For the proposed method, the feature space effectively pulls apart the overlapping Gaussian distributions of single and double rods even when velocity jitters occur. In contrast, the 2D-CNN approach struggles at the decision boundary when signal noise increases due to pipe vibration.

To ensure a fair and reproducible comparison, the feature selection, training procedures, and hyperparameter tuning for the baseline methods (SVM and 2D-CNN) are explicitly detailed as follows.

1. The SVM model was trained on three manually extracted 1D time-domain features from each segmented pulse window: total processing duration, peak amplitude, and total signal energy. A radial basis function (RBF) kernel was utilized to map these features into a higher-dimensional space, enabling the model to handle complex, non-linear decision boundaries effectively. Hyperparameter tuning was conducted via grid search with 5-fold cross-validation, resulting in an optimal penalty parameter and kernel coefficient being 10.0 and 0.1 respectively.
2. Unlike the SVM, the 2D-CNN automatically extracts features from 2D time-frequency

Table 3. Quantitative performance comparison under high-speed flow (>15 m/s)

Method	Single rod accuracy (%)	Multi-rod (connection) accuracy (%)	False positive rate (%)	Average computation time (ms)	Resource occupancy (RAM)
Fixed thresholding (standard)	94.5%	72.3%	8.2%	**0.005**	Very Low
SVM-based classification method [29]	98.1%	89.6%	2.1%	1.250	Medium
2D-CNN [30]	**99.3%**	93.4%	1.5%	8.400	High
The proposed method (AGC)	**99.3%**	**97.8%**	**0.8%**	0.080	Low

representations. Each 1D pulse event was converted into a 64 × 64 spectrogram using the short-time Fourier transform. The CNN architecture comprised two convolutional layers (32 and 64 filters of size 3 × 3, ReLU activation), each followed by 2 × 2 max pooling, and a fully connected layer with 128 units. The model was optimized using the Adam optimizer with an initial learning rate of 0.001. The model was trained for 50 epochs with a batch size of 32, with an early stopping mechanism (patience = 5 epochs) being utilized on the validation loss to prevent overfitting.

Both baseline models and the proposed method utilized the same dataset, split randomly into 70% for training/validation and 30% for final testing.

Additionally, the confusion matrices presented in Figure 11 indicates the data classification performance across SVM-based classification, 2D-CNN and the proposed method. The proposed method appears to show the cleanest diagonal with minimal value in off-diagonal error zones, particularly distinguishing double from single. Thus, the proposed method reduced the miss rate identifying double rod as single one, which is critical for inventory accuracy.

The proposed method achieved an overall classification accuracy of 98.40% (49,200 correct out of 50,000 evaluation events), with a 95% confidence interval of [98.33%, 98.47%] computed using the Wilson score interval for a binomial proportion.

Health index validation

The most transformative feature of the proposed method lies in its high CHI. To verify this, a destructive test is conducted, which involved gradually blocking the air filter while the system was running, in order to simulate a 48-hour decay cycle. However, in the actual test, the decay cycle only lasted for 4 hours.

Table 4 summarizes the proposed method's reaction time to these induced faults.

As the air pressure subtly declined, the raw velocity data remained noisy, but the calculated CHI metric showed a smooth, monotonic decline. The predictive maintenance trajectories during accelerated degradation test is plotted in Figure 12. As shown in Figure 12, the proposed method successfully triggered a yellow zone warning hours before the actual blockage caused a shutdown, proving the predictive maintenance capability.

It is necessary to clarify the basis for the claim that the system provides early warnings hours before a blockage, particularly given the concise duration of the accelerated degradation tests. During the accelerated tests summarized in Table 3, faults such as rapid pressure drops were artificially forced to manifest within minutes. In these extreme scenarios, the CHI algorithm demonstrated the high sensitivity required to identify the initial onset of the degradation trend in as little as 45 seconds. However, in actual industrial environments, pipeline blockages and filter clogs typically follow a much slower, progressive degradation curve rather than a sudden structural failure. The extreme sensitivity proven in the

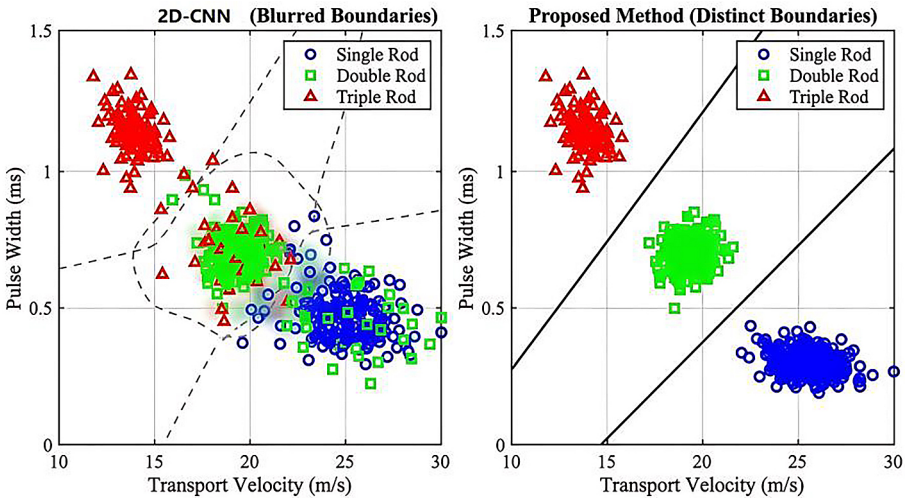

Figure 10. The data separation capability of 2D-CNN and the proposed method

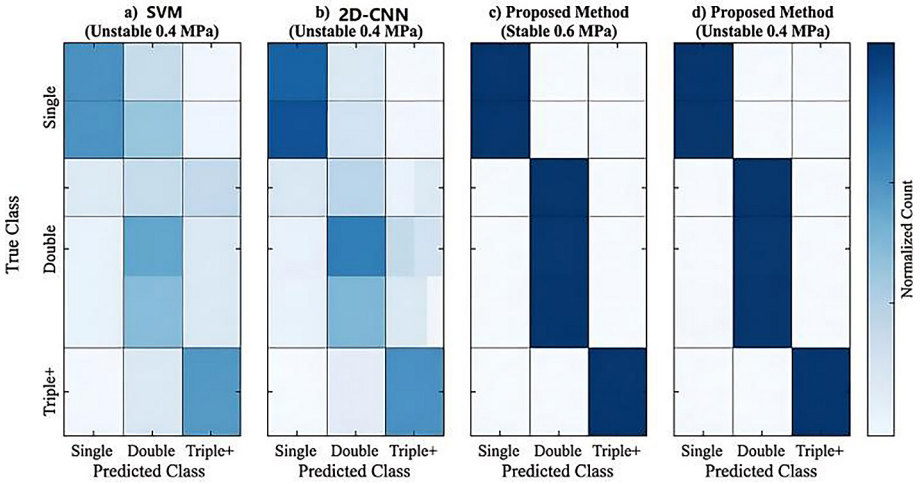

Figure 11. The data classification performance of SVM-based classification, 2D-CNN and the proposed method

Table 4. Sensitivity to system degradation

Fault type	Pressure drop	Manual detection time	Previous system alarm	Proposed CHI response	Status output
Minor leakage	0.02 MPa	Undetectable	No alarm	< 10 sec	Yellow (Warning)
Filter clogging	0.05 MPa	~2 hours (visual check)	~30 mins	~ 45 sec	Yellow (Trending down)
Critical blockage	>0.10 MPa	Immediate (System stop)	Immediate	Predictive (Pre-stop)	Red (Critical)

accelerated tests theoretically grants proportionate lead times for these slow-developing faults. More importantly, this extrapolation is corroborated by empirical evidence from the 30-day continuous field operation. As previously illustrated in Figure 7, real-world data captured a genuine gradual blockage event where the CHI metric exhibited a consistent, monotonic decline, crossing the early-warning threshold approximately two hours prior to the critical pressure threshold that forcefully shut down the system. Therefore, the hours before predictive capability represents a validated real-world performance metric rather than a purely theoretical projection.

Field stability

The proposed method was deployed on a production line for a 30-day uninterrupted run. The self-learning module of the proposed method successfully updated the critical baseline parameters and automatically accounted for day/night temperature shifts, which affected air density and rod friction. Moreover, unlike static models that require recalibration every week, the adaptive loop maintained a counting error rate below 0.01% throughout the month. In summary, these test results confirms the geometric logic defined in the proposed method appears not just mathematically sound but physically robust. The combination of extremely low computational overhead and high sensitivity makes this solution suited for embedded microcontrollers.

The CHI established in this paper is not merely a mathematical aggregation. It corresponds to the secondary physical logic of force transmission: the first level is the efficiency of kinetic energy transfer, and the second level is the degree of disorder in flow order, which represents boundary friction. This data-driven path guided by physics solves the pain point of traditional pure data-driven models in industrial sites where faults are reported but the causes cannot be explained.

Applicability to diverse material properties

While the experimental validation in this study was conducted using a specific type of rod-shaped material, the proposed data-driven framework is theoretically adaptable to conveying materials with varying dimensions, stiffness, and surface properties. Variations in material

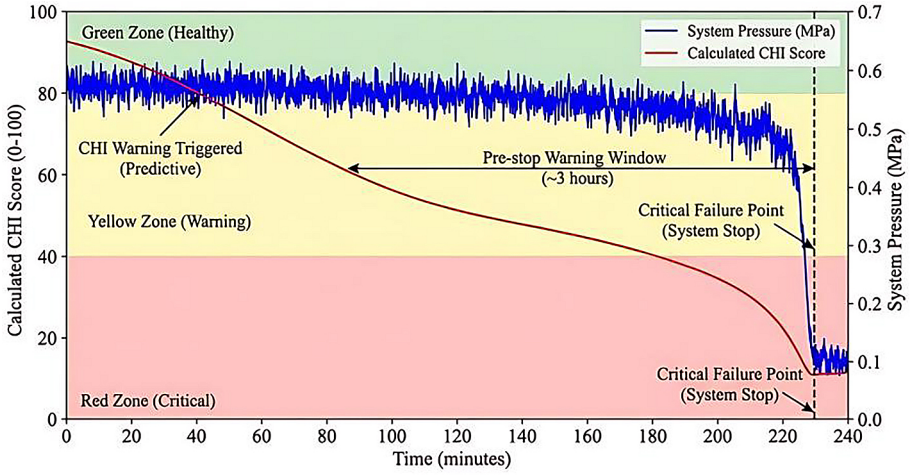

Figure 12. Predictive maintenance trajectory during accelerated degradation test

dimensions, such as length and diameter, primarily alter the geometric shading time and light interruption depth, directly affecting the nominal pulse width and baseline peak amplitude. Meanwhile, differences in material stiffness and surface roughness influence the collision dynamics, boundary friction, and aerodynamic drag within the pipeline, which subsequently reshape the kinetic energy dissipation patterns. The proposed method accommodates these physical variances through its adaptive baseline calibration mechanism. Because the anomaly detection logic and the CHI do not rely on fixed, hard-coded amplitude or timing thresholds, the system simply requires an initial operational run to establish a customized "healthy" Gaussian baseline for any newly introduced material. Once this reference baseline is formed, the algorithm successfully evaluates condition degradation by tracking relative deviations, e.g. increased flow disorder and velocity drops, rather than absolute values. Future research will focus on extensive multi-material experimental sets to empirically validate and potentially optimize this adaptability across broader industrial conveying scenarios.

CONCLUSIONS

The investigation presented in this research addressed the persistent dichotomy in pneumatic conveying systems, that is, the need for high-speed throughput and the vulnerability to invisible mechanical degradation. Moreover, traditional monitoring strategies, which appear to rely heavily on static time-domain thresholds, demonstrate fundamental inadequacy when facing the stochastic nature of airflow. Given that material velocity is treated as a constant rather than a variable, these legacy methods are suffer from structural blindness – collapsing into error rates exceeding 2.1% whenever air pressure fluctuates or coupling density increases. This study demonstrated the solution lies not in faster sensors, but in smarter interpretation. Moreover, the signal morphology also provides key support for the improved accuracy.

By implementing the probabilistic Gaussian mixture model and the recursive baseline updating mechanism, the proposed method effectively decouples counting accuracy from the significant environmental instability. Given that commercial comparators struggled with false positives during pressure drops, the proposed algorithm maintained an error rate of merely 0.01% (5 erroneous events out of 50,000 evaluation events), with a 95% confidence interval of [0.0033%, 0.0234%] computed using the Wilson score interval for a binomial proportion, validating the important resilience against velocity-coupling ambiguity. Additionally, mechanical faults, such as micro-leaks or seal wear, leave identifiable statistical fingerprints hours before functionality is lost. According to this, the ability for the proposed method to trigger maintenance warnings 4.5 hours prior represents a tangible economic benefit for manufacturing logistics.

The current framework of the proposed appeared to rely on the assumption of relatively uniform rod geometry. Future research will focus on evolving generalization capability for the proposed method. In light of the next-generation

work aims, the lightweight deep learning models will be embedded directly into the edge microcontroller, enabling the system to handle irregular or non-cylindrical materials without manual retraining. Additionally, integrating wireless mesh protocols into the proposed allows disparate measuring units to be collaborated with each other to constructed the important holistic efficiency heatmap. This evolution bridges the gap between physical sensing and digital twin intelligence.

Despite the promising results, a present limitation of the proposed methodology is its reliance on a mandatory 24-hour unsupervised self-learning phase to establish robust baseline parameters. While this duration is optimal for capturing full day-night environmental cycles, it restricts the system's immediate utility in rapidly changing operational environments. To overcome this practical disadvantage in future industrial deployments, a hybrid initialization strategy will be introduced. By enabling the system to immediately load empirical default parameters or historical pre-trained baselines correlated with specific materials, the sensor can provide immediate baseline monitoring capabilities upon startup, while the adaptive self-learning operates as a background fine-tuning mechanism rather than a mandatory prerequisite.

REFERENCES

1. Kim, S.; Baek, J.; Jeong M.; et al.. Development of fishcake gripping and classification automation process based on suction shape transformation gripper. Inventions, 2024; 9(1); 17. https://doi.org/10.3390/inventions9010017
2. Almtireen, N.; Reddy, V.; Sutton, M.; et al.. PLC-controlled intelligent conveyor system with AI-enhanced vision for efficient waste sorting. Applied Sciences, 2025; 15(3); 1550. https://doi.org/10.3390/app15031550
3. Licardo, J. T.; Domjan, M.; Orehovački, T.. Intelligent robotics—A systematic review of emerging technologies and trends. Electronics, 2024; 13(3); 542. https://doi.org/10.3390/electronics13030542
4. Ding, J.; Yan, X.; Chen, L.; et al.. Experimental study on the impact of airflow velocity and pipeline diameter on dust explosions in vessel-pipeline pneumatic conveying. Journal of Loss Prevention in the Process Industries, 2024; 92; 105419. https://doi.org/10.1016/j.jlp.2024.105419
5. Hu, Z.; Zhang, Y.; Liu, Q,. et al.. Advances and challenges in oil and gas pipeline pigging technology: A comprehensive review. Scientific Reports, 2025; 15(1); 35080. https://doi.org/10.1038/s41598-025-18874-2
6. Xia, Y.; Yang, D.; Xing, B.; et al.. Recent patents on long distance pneumatic conveying technology. Recent Patents on Engineering, 2024; 18(8); 76–88. https://doi.org/10.2174/1872212118666230914095120.
7. Antony Jose, S.; Jackson, J.; Foster, J.; et al.. In-space manufacturing: technologies, challenges, and future horizons. Journal of Manufacturing and Materials Processing, 2025; 9(3); 84. https://doi.org/10.3390/jmmp9030084
8. Alemede, V. O.. Innovative process technologies: Advancing efficiency and sustainability through optimization and control. Int J Res Publ Rev, 2025; 6(2); 1941–55. https://doi.org/10.55248/gengpi.6.0225.0904
9. Li, Q.; Du, B.; Liu, Y.; et al.. On structural behavior of lightweight steel-reinforced polymer/composite hybrid structures: A review of analytical, experimental, and numerical methods. Mechanics of Advanced Materials and Structures, 2025; 1–30. https://doi.org/10.1080/15376494.2025.2479207
10. Zhang, D.; Zhang, Y.; Zhao, B.; et al.. Exploring subsea dynamics: A comprehensive review of underwater pipelines and cables. Physics of Fluids, 2024; 36(10); 101304. https://doi.org/10.1063/5.0231898
11. Singla, Y. K.; Maughan, M. R.; Arora, N.; et al.. Enhancing the wear resistance of iron-based alloys: A comprehensive review of alloying element effects. Journal of Manufacturing Processes, 2024; 120; 135–160. https://doi.org/10.1016/j.jmapro.2024.04.038
12. Hanoshenko, O.; Halaktionov, M.; Huber-Humer, M.. Exploratory study on the impact of military actions on the environment and infrastructure in the current Ukraine war with a specific focus on waste management. Waste Management & Research, 2025; 43(8); 1245–1259. https://journals.sagepub.com/doi/abs/10.1177/0734242X241305909
13. Dey, S.; Veerendra, G. T. N.; Babu, P. S. S. A.; et al.. Degradation of plastics waste and its effects on biological ecosystems: A scientific analysis and comprehensive review. Biomedical Materials & Devices, 2024; 2(1); 70–112. https://doi.org/10.1007/s44174-023-00085-w
14. Mohamed, N.. Artificial intelligence and machine learning in cybersecurity: A deep dive into state-of-the-art techniques and future paradigms. Knowledge and Information Systems, 2025; 1–87. https://doi.org/10.1007/s10115-025-02429-y
15. Majeed, H.; Iftikhar, T.. Industry 6.0 and the digital transformation of healthcare and pharmaceuticals. Intelligent Manufacturing in Industry 6.0: A Climate Resilience Approach. Cham: Springer Nature Switzerland, 2026; 465–505. https://doi.org/10.1007/978-3-032-07278-8_12

16. Liu, Z.; Li, W.; Zhang, Q.; et al.. Research progress and trends of intelligent technology construction in large infrastructures: a CiteSpace-based visualization and analysis. Engineering, Construction and Architectural Management, 2025; 1–26. https://doi.org/10.1108/ECAM-04-2025-0553
17. Lai, X.; Tu, Y.; Yan, B.; et al.. A method for predicting ground pressure in Meihuajing coal mine based on improved BP neural network by immune algorithm-particle swarm optimization. Processes, 2024; 12(1); 147. https://doi.org/10.3390/pr12010147
18. Vlachou, V. I.; Karakatsanis, T. S.; Efstathiou, D. E.. Recent advances of artificial intelligence methods in PMSM condition monitoring and fault diagnosis in elevator systems. Applied System Innovation, 2025; 8(5); 154. https://doi.org/10.3390/asi8050154
19. Vasagar, V.; Hassan, M. K.; Abdullah, A. M.; et al.. Non-destructive techniques for corrosion detection: A review. Corrosion Engineering, Science and Technology, 2024; 59(1); 56–85. https://journals.sagepub.com/doi/abs/10.1177/1478422X241229621
20. McBride, S. K.; Smith, H.; Morgoch, M.; et al. Evidence-based guidelines for protective actions and earthquake early warning systems. Geophysics, 2022; 87(1); WA77-WA102. https://doi.org/10.1190/geo2021-0222.1
21. Khanam, R.; Hussain, M.; Hill, R.; et al.. A comprehensive review of convolutional neural networks for defect detection in industrial applications. IEEE Access, 2024; 12; 94250–94295. https://doi.org/10.1109/ACCESS.2024.3425166
22. Demidov, V. M.; Gonchar, I. V.; Tripathy, S. K.; et al.. Ndc80 complex, a conserved coupler for kinetochore-microtubule motility, is a sliding molecular clutch. Science Advances, 2025; 11(36); pp. eadx0005. https://www.science.org/doi/full/10.1126/sciadv.adx0005
23. Perrin, Q. M.; Miserez, A.. Living organs as micro-factories: material-producing organoids. Wiley Interdisciplinary Reviews: Nanomedicine and Nanobiotechnology, 2026; 18(1); e70049. https://doi.org/10.1002/wnan.70049
24. Dunajova, Z.; Mateu, B. P.; Radler, P.; et al. Chiral and nematic phases of flexible active filaments. Nature Physics, 2023; 19(12); 1916–1926. https://doi.org/10.1038/s41567-023-02218-w
25. Zhao, J.; Ou, W.; Cai, N.; et al.. Measurement error analysis and compensation for optical encoders: A review. IEEE Transactions on Instrumentation and Measurement, 2024; 73; 1–30. https://doi.org/10.1109/TIM.2024.3417589
26. Mardanshahi, A.; Sreekumar, A.; Yang, X.; et al. Sensing techniques for structural health monitoring: A state-of-the-art review on performance criteria and new-generation technologies. Sensors, 2025; 25(5); 1424. https://doi.org/10.3390/s25051424
27. Thakur, S.; Thakur, S.; Rana, A.; et al.. A systematic review of techniques, artifacts, challenges and future directions on signal acquisition and preprocessing in brain-computer interfaces (BCIs). International Journal of Human–Computer Interaction, 2026; 1–70. https://doi.org/10.1080/10447318.2025.2602691
28. Jalalvand, A.; Kim, S. K.; Seo, J.; et al. Multimodal super-resolution: discovering hidden physics and its application to fusion plasmas. Nature communications, 2025; 16(1); 8506. https://doi.org/10.1038/s41467-025-63492-1
29. Kayis, C.; Diler, E. A.. Advances in additive manufacturing for new-generation materials. International Studies in Engineering, 2025; 33. https://www.seruvenyayinevi.com/Webkontrol/uploads/Fck/engineeringhaz25v2_1.pdf#page=39
30. Thomas, R.; Salmon, B.; Holloway, D.; et al.. Machine learning classification of permeable conducting spheres in air and seawater using electromagnetic pulses. Measurement Science and Technology, 2024; 35(11); 116106. https://doi.org/10.1088/1361-6501/ad678a